



The coupling of winds, ocean turbulence, and High Salinity Shelf Water in the Terra Nova Bay Polynya



Una Kim Miller^{a,*¹}, Christopher J. Zappa^a, Arnold L. Gordon^a, Seung-Tae Yoon^b, Craig Stevens^{c,d}, Liv Cornelissen^{c,d}, Sukyoung Yun^e, Won Sang Lee^e

^a Lamont Doherty Earth Observatory of Columbia University, NY, USA

^b Kyungpook National University, Daegu, South Korea

^c National Institute of Water and Atmospheric Research, Wellington, New Zealand

^d University of Auckland, Auckland, New Zealand

^e Korea Polar Research Institute, Incheon, South Korea

ARTICLE INFO

Handling Editor: Dr W Smith

ABSTRACT

The Terra Nova Bay (TNB) Polynya in the Western Ross Sea of Antarctica is a major producer of High Salinity Shelf Water (HSSW), a precursor to Antarctica Bottom Water (AABW). Processes occurring in and around the polynya can therefore effect change in the lower limb of overturning circulation in this region. Here, we use data from a densely-instrumented upper-ocean mooring, deployed for 1 year in a region of active HSSW formation within TNB, to examine the coupling of surface brine rejection and vertical mixing to katabatic wind forcing. We find a high correlation between salinity and winds during the wintertime HSSW production season at the mooring site, with a lag-response of 20 h in near-surface (~47 m) salinity to winds measured at the nearby Automatic Weather Station (AWS) Manuela. Salinity and temperature measurements show a fully destratified water column by June, with a lag-response of near-seabed (~360 m) salinity to near-surface salinity of just 5 h. Measurements of turbulent kinetic energy (TKE) dissipation rate (ϵ) from moored pulse-coherent acoustic Doppler current profilers (ADCPs) show general agreement with classic boundary layer scaling (BLS), and calculations of a vertical mixing timescale using the Obukhov length scale average to ~2.5 h during austral winter, consistent with the 5-h lag time observed in the salinity data. Comparisons to data from concurrent mooring deployments along the southern boundary of TNB, as well as to previously published assessments of model simulations and data from Climatic Long-term Interaction for the Mass-balance in Antarctica (CLIMA) moorings, allow us to explore spatial variability in the coupling of winds and salinity across TNB and to speculate on possible HSSW circulation pathways.

1. Introduction

The Terra Nova Bay (TNB) Polynya in the western Ross Sea of Antarctica was described in the early 20th century by Scott's Northern Party (Bromwich and Kurtz 1982), who noted a persistent open water area in the bay tied to strong winds blowing from the Reeves Glacier. The polynya has been studied since with satellite imagery (e.g. Aulicino et al. 2018; Bromwich, 1989; Ciappa and Budillon 2012; Parmiggiani 2006; van Woert et al., 2001), ship-based observations (e.g., Ackley et al., 2020; Thompson et al. 2020; Guest, 2021a,b), numerical models (e.g., Xu et al. 2023a; Kim et al., 2023; Mathiot et al. 2012) and mooring

programs, such as the Italian National Program for Antarctic Research (PNRA) Climatic Long-term Interaction for the mass balance in Antarctica (CLIMA) project (Gordon et al., 2004; Gordon et al. 2009; Spezie and Manzella, 1999). Yet, relatively few in-situ measurements have been collected during the inhospitable austral winter months, when the polynya forms and produces a critical water mass known as High Salinity Shelf Water (HSSW). HSSW production results from the extreme forcing of katabatic winds, which occur when cold, dense air masses capable of reaching speeds upwards of 50 m^{-1} descend from the Antarctic Ice Sheet to the sea through glacial channels. Katabatic winds can persist continuously for days to weeks, pushing sea ice away from

* Corresponding author.

E-mail address: una.miller@uri.edu (U.K. Miller).

¹ Current affiliation: University of Rhode Island, RI, USA.

shore and thereby forming and maintaining coastal polynyas. The ensuing ocean-to-atmosphere heat loss supports conditions of intensive and continuous sea ice production within the polynya, and the associated brine rejection feeds reservoirs of dense water at depth, forming new HSSW. Despite being approximately 1/8 the size on average of its neighboring Ross Sea Polynya to the south (Martin et al. 2007), the TNB Polynya produces an estimated 1/3 of total HSSW volume in the Ross Sea (Jendersie et al., 2018; Mathiot et al. 2012), as well as the most saline variety of HSSW across Antarctica, with salinities exceeding 34.8 (Orsi and Wiederwohl 2009). Its year-average production rate was estimated to be on the order of 0.4 Sv in the past decade, with strong sub-seasonal variability tied to the katabatic wind regime (Miller et al. 2024). HSSW formed in the highly wind-forced surface layer along the front of the Nansen Ice Shelf (Mathiot et al. 2012; Miller et al. 2024) drains into the Drygalski Basin and travels through the Drygalski Trough to the continental shelf break (Gordon et al. 2009; Jendersie et al., 2018). Over the course of this journey, HSSW mixes with Ice Shelf Water (ISW) and modified Circumpolar Deep Water (mCDW) to become the Ross Sea variety of Dense Shelf Water (DSW), which exits the shelf break in tidally-modulated gravity plumes to become AABW (Gordon et al. 2009; Bowen et al. 2023; Wang et al., 2013). Therefore, HSSW produced in TNB directly feeds and influences Antarctic Bottom Water (AABW) in the Pacific- and Australian-Antarctic basins.

For decades, the Ross Sea, and in particular TNB (Castagno et al. 2019), has been observed freshening due to increased glacial meltwater advected in from the Amundsen and Bellinghauses Seas to the east (Jacobs et al., 2022), which in turn has driven a freshening and contraction of downstream AABW evident in observations spanning 1970 to the early 2010's (Gordon et al., 2015; Purkey et al., 2019; Purkey and Johnson, 2012). This persistent trend was recently interrupted by a period of rebounding salinity, in which weakened easterly winds in 2015–2018 reduced the import of sea ice into the Ross Sea from

the Amundsen Sea, resulting in greater in-situ production of sea ice across the Ross Sea. Increased brine rejection increased the salinity of HSSW produced in the TNB polynya, temporarily restoring the salinity, density, and thickness of downstream AABW to values approaching those last observed in the 90's (Castagno et al. 2019; Silvano et al. 2020). While the impact of such regional processes on HSSW and downstream AABW is clear, relatively few in-situ austral wintertime observations are available to examine how polynya-and smaller-scale dynamics modulate the properties and production rates of HSSW. Moorings allow for continuous in-situ data collection during the winter months when HSSW is formed, but are often sparsely instrumented in the upper ocean, where brine rejection and the vertical mixing of cold, salty surface waters to depth occur — two key aspects of the HSSW formation process. Here, we use data from three moorings deployed for a 1-year period in TNB to examine the timescales, turbulent mixing, and possible transport pathways of HSSW in TNB in response to katabatic wind forcing. The "Lamont-Doherty Earth Observatory (LDEO) mooring", previously described in Miller et al. 2024, was deployed in the upper ocean near the Nansen Ice Shelf, a region of active HSSW formation within the bay (Fig. 1). Two additional moorings were deployed along the northern flank of the Drygalski Ice Tongue (DIT): the "Drygalski Ice Tongue Deep (DITD) mooring", deployed within the Drygalski Basin, which channels HSSW flowing out of the bay, and the "Drygalski Ice Tongue North (DITN) mooring", deployed in the southeast corner of the bay (Fig. 1). We focus on several key questions: (1) Is there spatial variability in brine rejection across TNB in response to katabatic wind forcing? (2) What is the nature of turbulence associated with katabatic wind forcing and HSSW production? and (3) How do these mooring observations augment the current understanding of pathways for HSSW circulation within TNB?

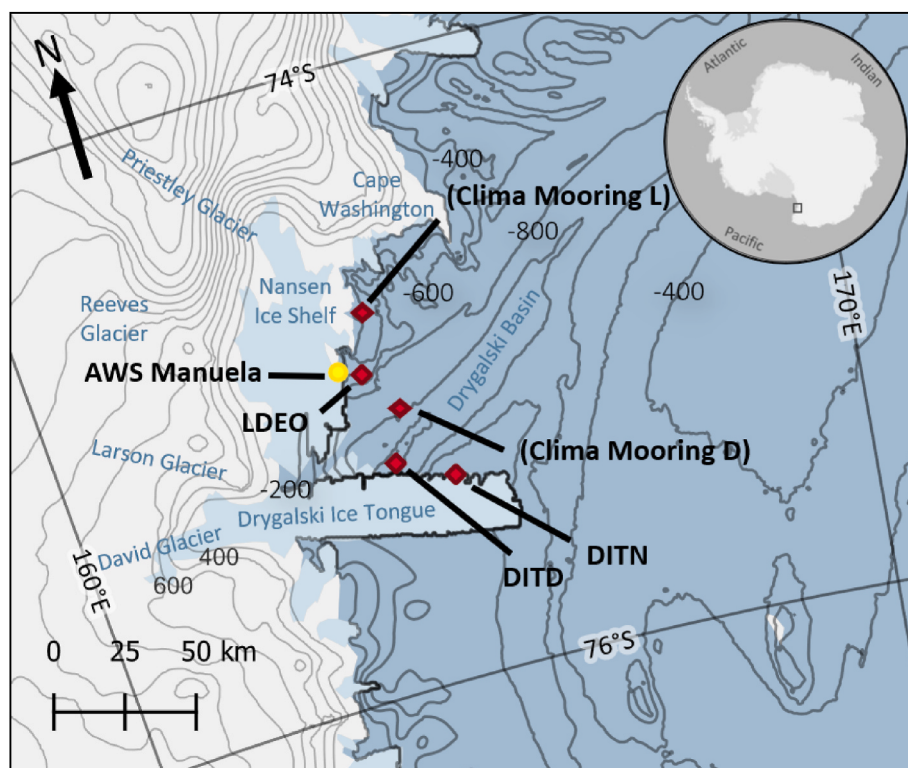


Fig. 1. Locations of referenced datasets in Terra Nova Bay. Data analyzed in this study were collected from the Automatic Weather Station (AWS) Manuela and the Lamont-Doherty Earth Observatory (LDEO), Drygalski Ice Tongue Deep (DITD) and Drygalski Ice Tongue North (DITN) moorings. Moorings labeled in parentheses, Climatic Long-Term Interactions for the Mass-balance in Antarctica (CLIMA) moorings D (1995–2003) and L (2007), were analyzed and discussed by Rusciano et al. 2013, Yoon et al. 2020, and Le Bel et al. 2021. The basemap asset shown here is made available by Matsuoka et al. 2021.

2. Data and methods

2.1. Mooring data

The LDEO mooring was deployed in February 2017 and recovered in March 2018 at -74.97° , 163.96° (Fig. 1). It was situated approximately 7 km to the east of the Nansen Ice Shelf in 390 m water depth, on a local bathymetric high roughly 4 km by 4 km in area and directly in the pathway of the defining katabatic wind pathway in TNB (the Reeves Glacier; Ciappa et al. 2012). Instrumentation used in this study include i) seven temperature-conductivity sensors across the full water column depth of the mooring, ii) two pulse-coherent acoustic Doppler current profilers (ADCPs) at 47 m and 85 m, and iii) three current meters at depths of 230, 292, and 364 m (Table 1). Pulse-coherent ADCPs transmit two consecutive acoustic waves, or "pulse pairs", at a known time lag and record the phase shift between the reflected pulses, which provides information on local velocity at a much finer scale than do typical single-pulse ADCPs. The resulting finescale velocity profiles (less than 2 m in range and with bin sizes on the order of cm) may be used to estimate turbulent kinetic energy (TKE) dissipation rates (ε). The ADCPs were programmed to sample in bursts, collecting 530 profiles at 8 Hz once every hour, using a single transducer facing away from the mooring line and oriented at a 45° angle upwards relative to the horizontal plane orthogonal to the instrument axis.

Two additional moorings were deployed concurrently to the LDEO mooring by the National Institute of Water and Atmospheric research (NIWA) (Yoon et al. 2020; Stevens et al., 2024): the DITD mooring in the southern Drygalski Basin at -75.28° , 164.06° in 1300 m water depth and the DITN mooring at -75.36° , 164.75° in 690 m water depth (Fig. 1). Instrumentation included temperature-conductivity sensors at 1224 m depth on DITD and at 75, 275, and 675 m on DITN, and current meters at 1239 m on DITD and 694 m on DITN (Table 1). Horizontal current directions from all moorings were corrected for magnetic declination. Potential temperature, practical salinity, and potential density were calculated using the Gibbs-SeaWater Oceanographic Toolbox (GSW) (McDougall and Barker, 2011).

Table 1

Moored instrumentation used in the present study. The Lamont-Doherty Earth Observatory (LDEO) mooring was located at -74.97° , 163.96° , near the Nansen Ice Shelf. Drygalski Ice Tongue North (DITN) and Deep (DITD) were located at -75.36° , 164.75° and -75.28° , 164.06° E, respectively. Moorings were deployed from February 2017 to March 2018. The temperature-conductivity sensors are manufactured by Seabird Electronics (SBE), with asterisked depths indicating pumped models. Here, ε is the dissipation rate of turbulent kinetic energy (TKE).

Instrument	Depth [m]	Data	Sampling Rate
LDEO			
SBE37 SM(P)-37	47*, 95*, 119, 144, 168, 219, 360	Conductivity and temperature	$*1 \text{ min}^{-1}$, 2 min^{-1}
DITN			
2-Mhz Nortek AquaDopp High-Resolution (HR) current profiler	47, 85	Turbulence (ε)	1 h^{-1}
Nortek AquaDopp current meters	230, 292, 364	Current velocity	1 min^{-1}
DITD			
SBE37 SM-37	75, 275, 675	Conductivity and temperature	1 min^{-1}
Nortek AquaDopp current meter	694	Current velocity	1 min^{-1}
DITD			
SBE37 SM-37	1224	Conductivity and temperature	1 min^{-1}
Nortek AquaDopp Current meter	1239	Current velocity	1 min^{-1}

2.2. Meteorological forcing

Automatic Weather Station (AWS) Manuela is located at -74.95° S, 163.68° on Inexpressible Island, a small island at the edge of the Nansen Ice Shelf and in the katabatic wind pathway constrained by the Reeves Glacier. Measurements at 10-min frequency included wind speed and direction, and atmospheric temperature, pressure, and humidity. Instruments are reported to be roughly 2.1 m above the ground. Data were downloaded for the time period of the mooring deployment, February 2017–March 2018. Wind stress (τ) at the ocean surface and water-side friction velocity, $u_* = \sqrt{\tau/\rho}$, were calculated using the COARE bulk flux algorithm (Fairall et al., 1996; Fairall et al., 2003), with the input wind from AWS Manuela divided by a factor of 1.5 to account for attenuation across the distance from the AWS to the mooring (Miller et al. 2024; Rhee et al. 2022).

Buoyancy flux at the surface, B_0 , was calculated as

$$B_0 = -(gaQ_{\text{net}})/(\rho_0 c_p) + g\beta(E - P)S_0 \quad (1)$$

where g is gravity, α is the thermal expansion coefficient, Q_{net} is net surface heat flux (positive upward), ρ_0 is surface ocean potential density (approximated using ρ_0 at the 47 m sensor on the LDEO mooring), c_p is the specific heat of water, β is the haline contraction coefficient, E and P are the rates of evaporation and precipitation, and S_0 is the surface salinity (approximated using salinity at the 47 m sensor). The shortwave, longwave, sensible, and latent components of Q_{net} were parameterized as in Miller et al. 2024, using wind speeds from AWS Manuela and all other parameters from the single-level European Center for Medium-Range Weather Forecasts (ECMWF) Re-Analysis 5 (ERA5) at a 6-h time step and 0.25° by 0.25° spatial grid. The heat transfer coefficient for latent and sensible heat fluxes was set to 1.75×10^{-3} following similar calculations in TNB (Fusco et al. 2009; Budillon et al. 2000), though a range of coefficients may be argued to be suitable for the polynya environment (Miller et al. 2024).

2.3. Calculation of turbulent kinetic energy dissipation rate

Finescale velocity profiles from the two pulse-coherent ADCPs were processed and used to estimate ε following the methods described by Zippel et al., (2021). Individual pings with correlation values (the normalized amplitude of the auto-correlation function of the pulse pairs generated and received by the instrument) lower than 65% and entire profiles with averaged correlation values lower than 70% were removed. Measurements of ε were calculated from the wavenumber power spectra ($E(k)$) in the inertial subrange of turbulence according to the following relationship (Zippel et al., 2021), based on Kolmogorov's "-5/3 power law" (Kolmogorov, 1941),

$$E(k) = G(k, L_T, L_R) \left(C \epsilon^{2/3} k^{-5/3} + N \right) \quad (2)$$

where $G(k, L_T, L_R)$ is an instrument transfer function that accounts for the spatial sampling filter resulting from the near-rectangular sampling windows of the instrument's transmit and receive pulses, of lengths L_T and L_R , respectively, $C = 0.53$ (Sreenivasan 1995), k is wavenumber, and N is instrument noise that causes a spectrum to deviate from the theoretical $-5/3$ wavenumber exponential decay. $E(k)$ and k are measured, $G(k, L_T, L_R)$ is calculated, and ϵ and N are solved for by least-squares fitting of the measured spectrum to equation (2).

3. Results

3.1. Response of near-surface salinity to winds

To examine the response of near-surface salinity at the LDEO mooring site to katabatic winds, we calculate Pearson's correlation coefficient (R) between time-lagged wind speeds at AWS Manuela and the

shallowest (47 m) salinity measurements at the LDEO mooring:

$$R = \frac{\sum (x - \bar{x})(y - \bar{y})}{\sqrt{\sum (x - \bar{x})^2} \sqrt{\sum (y - \bar{y})^2}} \quad (3)$$

where x is a 30-day window of practical salinity and y is a sliding, time-lagged 30-day window of nominal wind speeds at AWS Manuela. Both the salinity- and wind-speed-windows are linearly detrended prior to calculation of R . The salinity-window is incremented forward in time by intervals of 1 day (e.g., the y-axis in Fig. 2a), such that the first window encompasses data between February 15 through March 16, the second window encompasses data between February 16 through March 17, and so on. Correlation is calculated between each salinity-window and a sliding wind-speed-window incremented by 1 h starting from 500 h preceding the salinity-window (negative lag) to 500 h proceeding the salinity-window (positive lag) (e.g., the x-axis in Fig. 2a). Values of R above a 95% significance level calculated for each of the salinity-windows with each of the time-lagged wind-speed-windows are shown in Fig. 2a. Near-surface salinity appears to couple strongly to negatively-lagged wind speeds from April through September, with R values exceeding 0.6 in April and again from June through August at lag times of around -20 h (e.g., Fig. 2b). Weaker peaks in negative and positive R occurring at both positive and negative lag times are also observed; these arise from 1–2-week periodicities present in both the salinity and wind signals such that the lagged wind speed signal falls in phase (positive peaks) and out of phase (negative peaks) with salinity at multiple lag times. In contrast, an identical lag-correlation analysis of winds at AWS Manuela and near-surface (75 m) salinity at DITN yield no strong negative nor positive correlations (not shown).

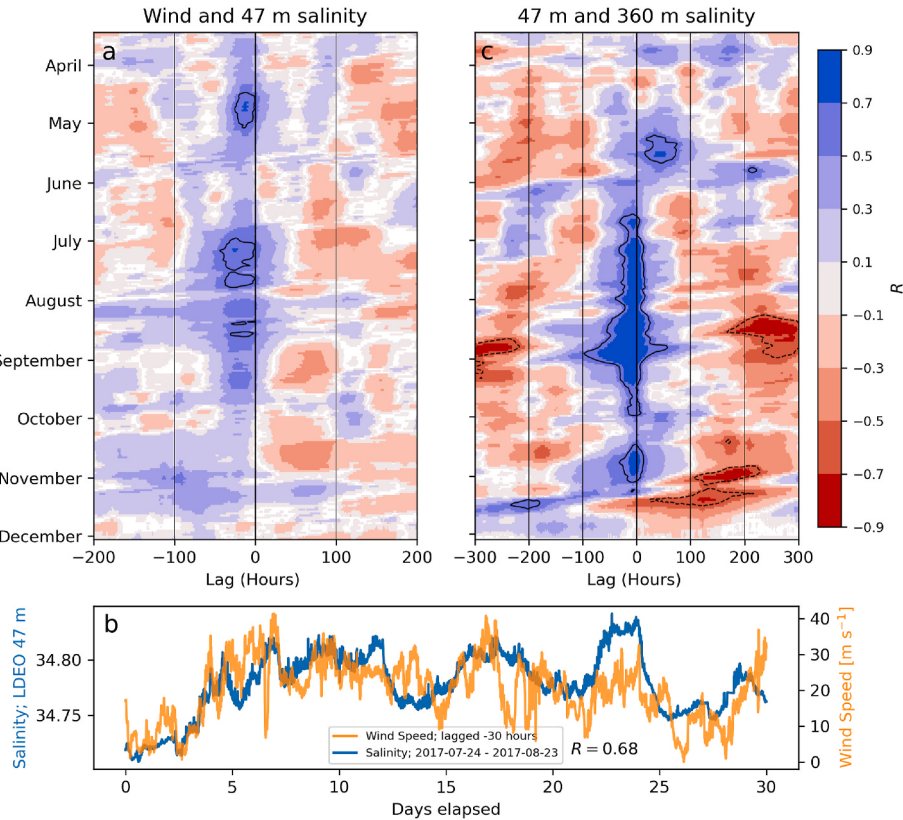


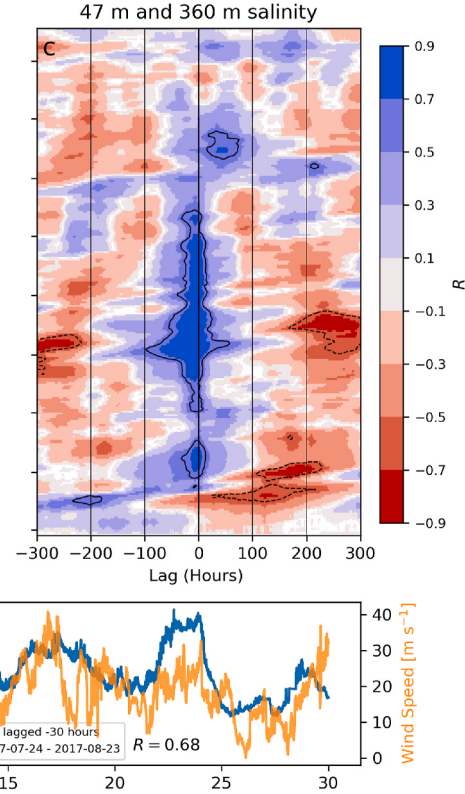
Fig. 2. Sliding time-lag correlations across the mooring deployment period between (a) nominal wind speeds at Automatic Weather Station (AWS) Manuela and the shallowest (47 m) salinity measurements on the LDEO mooring, with (b) an example of highly-correlated time series pair, and (c) the shallowest (47 m) and deepest (360 m) salinity measurements on the LDEO mooring. For each pairing, sliding 30-day windows of one variable (wind speed in Panel a and salinity at 47 m in Panel c) are iteratively time-lagged before and after a fixed 30-day window of the other variable (salinity at 47 m in Panel a and salinity at 360 m in Panel c) across the full range of hours shown on each x-axis. The time indicated on the y-axes of Panels a and c is the start date of each fixed 30-day window. White spaces (distinct from the light pink indicating $|R| < 0.1$) denote time series pairs that did not produce a value of R above a 95% significance level. Black contours indicate $|R| > 0.6$.

3.2. Propagation of the salinity signal to depth

We next examine the propagation of the near-surface brine rejection signal to depth, the mechanism by which HSSW is produced. Lagged correlations are calculated on linearly-detrended, 30-day data windows of salinity at 47 m and salinity at each of 95, 119, 144, 168, 210, and 360 m on the LDEO Mooring. Correlations significant to the 95% level between 47 m and 360 m are shown in Fig. 2c and correlations between 47 m and all measured depths are shown averaged across five sequential 60-day periods in Fig. 3. As with correlations between wind and salinity at 47 m, correlations between salinity at 47 m and salinity deeper on the mooring line exhibit a seasonal shift in both lag times and strengths of correlation. In February through May, correlation strength decreases with depth and the peak in correlation between 47 m and 360 m lags far behind that of other depths at nearly -40 h (Fig. 3a). This indicates that vertical mixing of brine produced at the surface to depth is inhibited by strong seasonal water column stratification during the late summer months. Correlation strength between the near-surface and depth increases as the season progresses and stratification is broken down, reaching its maximum in the June through August period with values exceeding 0.8 at all depths (Fig. 3c). The lag time at 360 m decreases to an average of roughly 5 h, the shortest lag time at that depth observed across the year. By the October through December period (Fig. 3e), austral summer, stratification begins to reestablish and correlations again exhibit a strong decay with depth.

3.3. Turbulence scaling

In the intensely wind-forced environment of a coastal polynya, tur-



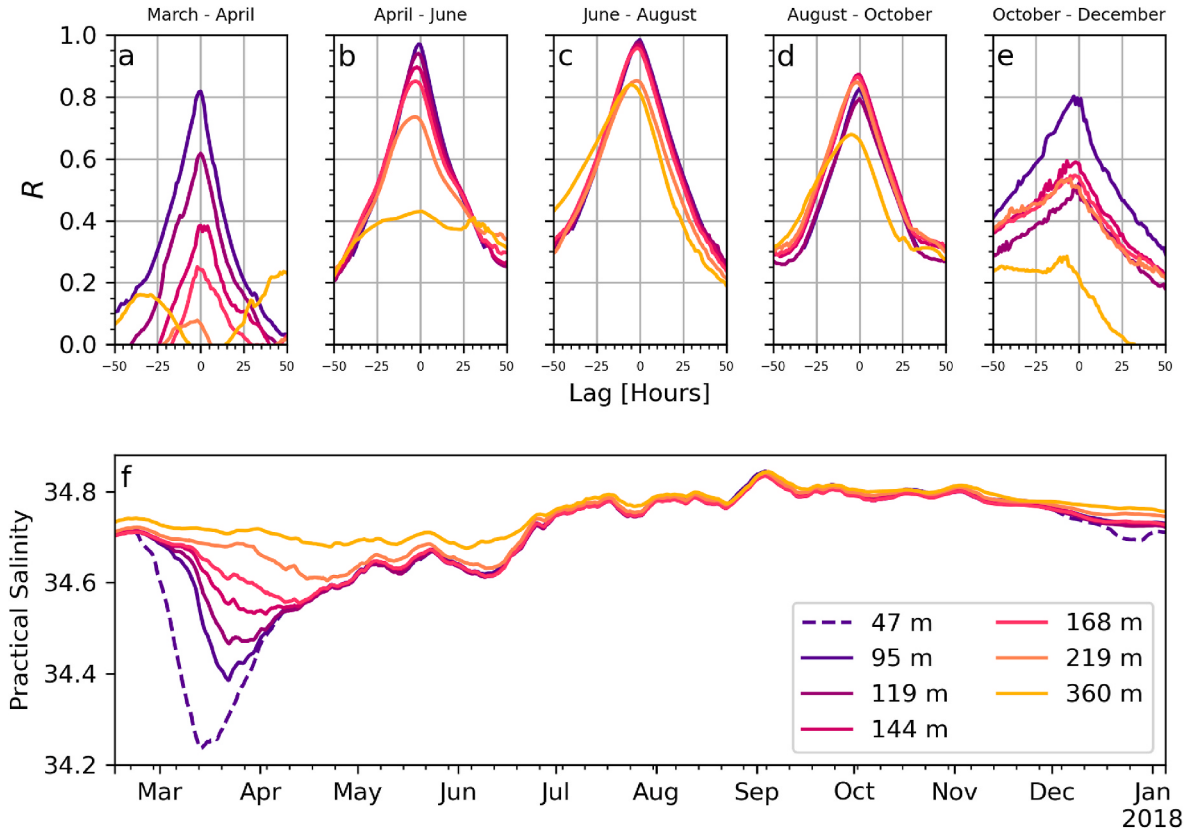


Fig. 3. The evolution of water column stratification at the LDEO mooring site. a-e) Lagged correlations between 30-day windows of salinity at 47 m on the LDEO mooring with time-lagged 30-day windows of salinity measured at each of the deeper sensors, averaged within 60-day seasonal time bins. f) The time series of salinity across all 7 depths as rolling 10-day means.

bulent mixing is undoubtedly central to understanding water column structure and fluxes. Turbulence can be quantified through measurements of ϵ , which is the rate of dissipation of TKE into heat energy. In the absence of 3D effects, the loss of TKE by viscous dissipation is balanced by the sum of its production (P) by shear stress, convection, and/or wave-processes, i.e., $P \approx \epsilon$. Thus, measurements and scaling of ϵ provide valuable information on the sources and magnitude of turbulent mixing in an environment. In conditions dominated by wind-driven mixing ("wind-dominant"), ϵ is expected to scale according to the classic law of the wall (LOW),

$$\epsilon = \frac{u_*^3}{\kappa|z|} \quad (4)$$

where u^* is ocean-side friction velocity, κ is the von Kármán constant, and z is the depth of the measurement. In buoyancy-driven mixing conditions ("buoyancy-dominant"), ϵ simply scales to surface buoyancy flux,

$$\epsilon = B_0 \quad (5)$$

Conditions of wind-dominant or buoyancy-dominant forcing are determined with the Obukhov length scale (L_M),

$$L_M = \frac{u_*^3}{\kappa B_0} \quad (6)$$

Conceptually, L_M in the ocean defines a depth down to which wind-driven turbulence is dominant. Below this depth, convective turbulence is dominant. Thus, LOW (Equation (4)) is valid where $|z/L_M| \ll 1$ and Equation (5) is valid where $|z/L_M| \gg 1$. Note that the inequalities are defined as "much greater than" and "much less than" unity. This is because where $z \approx L_M$, both wind-driven and convective turbulence are

important and a combination of LOW and Equation (5) is expected to apply (Lombardo and Gregg, 1989). In practice, the inequalities used to distinguish the wind-driven and convective turbulence regimes are typically around $|z/L_M| < 0.5$ for the former and $z/L_M < -5$ for the latter (e.g., Miller et al., 2023; Zippel et al., 2021). In this study, we define a looser threshold for the convective regime of $z/L_M < -3$ due to a limited number of data points in these conditions. Equations (4)–(6) fall under what is known as classic boundary layer scaling (BLS), and form the basis for the widely-used Monin-Obukhov Similarity Theory. Excluded from classic BLS are conditions of breaking waves, Langmuir circulation (e.g., Gordon 1970), and strongly stratifying surface buoyancy fluxes ($B_0 \gg 0$).

We first examine turbulence measured at the LDEO mooring in the context of the katabatic wind regime. Wind speed measured at AWS Manuela exhibits distinct seasonality, with strong, katabatic winds and occurring between February through October (austral fall/winter), followed by low winds from October onward (Fig. 4a). This drives water column destratification and restratification, as observed in calculations of mixed layer depth from moored temperature and salinity (Fig. 4b). This seasonality is reflected in the time series of ϵ at both 47 (Fig. 4c) and 85 m (Fig. 4d), which show elevated turbulence at both depths during the katabatic wind season, with values on the order of $10^{-6} \text{ W kg}^{-1}$, compared to values on the order of $10^{-8} \text{ W kg}^{-1}$ during the austral spring/summer months. More than 70% of hourly ϵ measurements across the entire deployment period of February 2017 through February 2018 occur under wind-dominant conditions of $|z/L_M| < 0.5$. Accordingly, values of $u^3/\kappa z$ (yellow and green dashed lines) are similar to measurements of ϵ across the whole study period at both depths.

To directly examine the performance of LOW and Equation (5), we show measurements of ϵ plotted directly against $u^3/\kappa z$ in wind-dominant conditions and plotted directly against B_0 in buoyancy-dominant

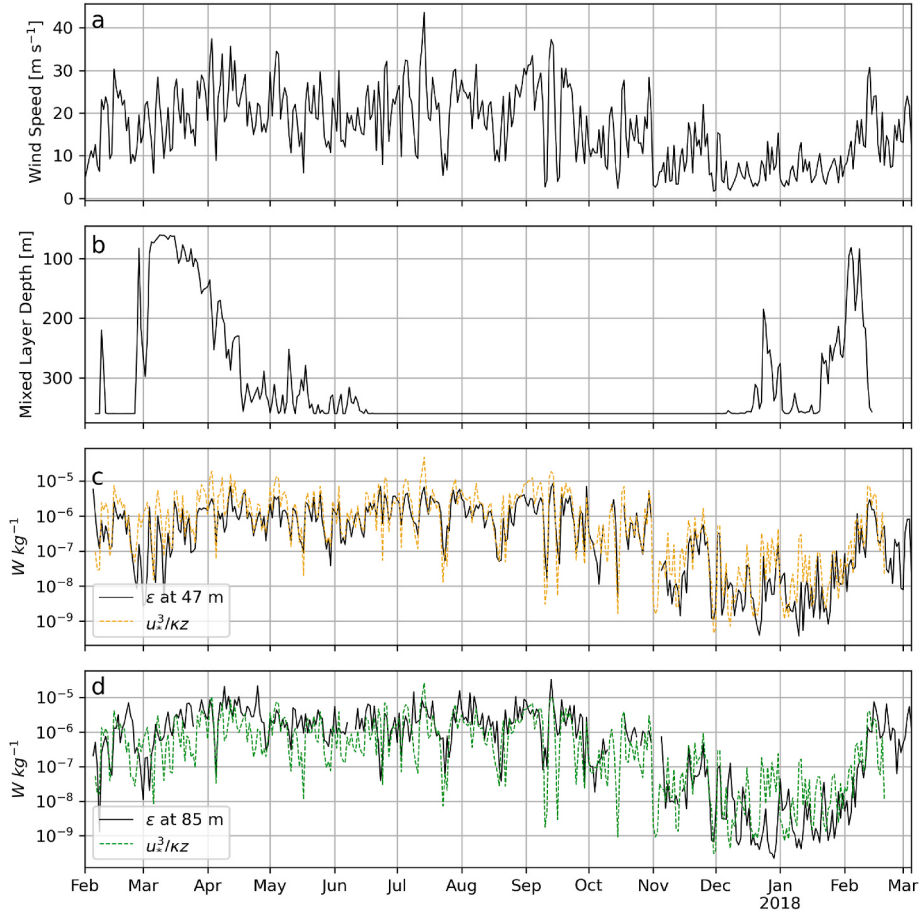


Fig. 4. a) Daily-averaged nominal wind speed measured at Automatic Weather Station (AWS) Manuela. b) Daily-averaged mixed layer depth, defined as the depth at which potential density (interpolated across the mooring temperature-salinity sensors) differs by 0.03 kg m^{-3} from the shallowest measurements at 47 m. The mixed layer depth calculation bottoms out at 360 m, the depth of the deepest temperature-salinity sensor, though the water depth at the mooring site is 390 m. c) Daily-averaged time series measurements of turbulent kinetic energy (TKE) dissipation rate (ϵ) at 47 m with daily-averaged predictions of ϵ according to the Law of the Wall (Equation (4)) overlaid in yellow. d) As in Panel c, but at 85 m.

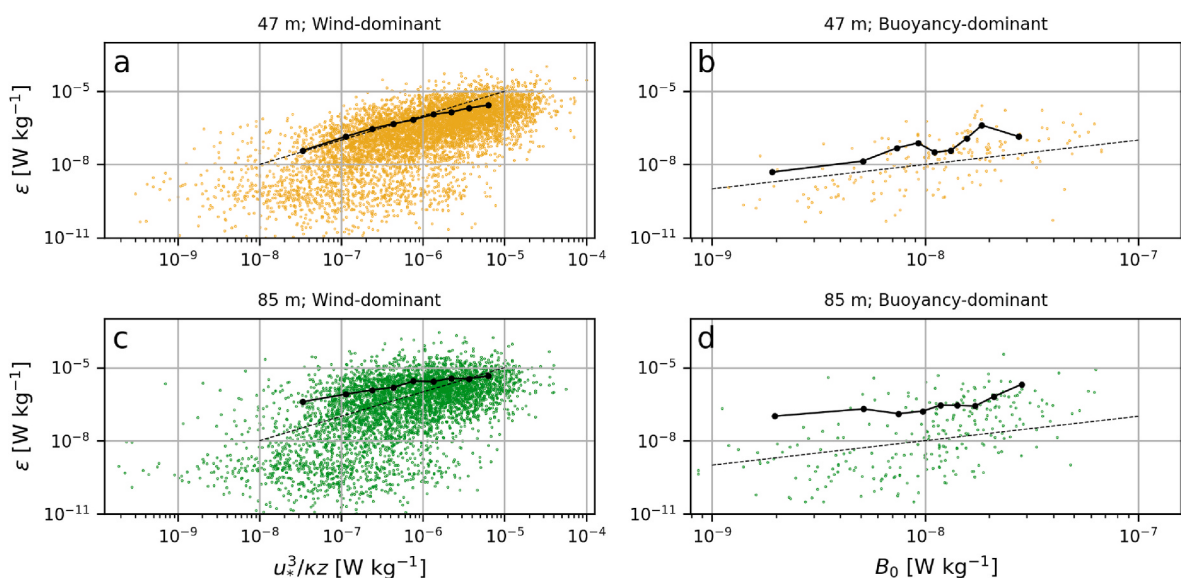


Fig. 5. Direct comparison of ϵ in wind-dominant conditions ($|z/L_M| < 0.5$) to values predicted according to Law of the Wall (LOW; Equation (4)) at a) 47 m and b) 85 m. Direct comparison of ϵ in buoyancy-dominant conditions ($z/L_M < -3$) against values predicted by Equation (5) at c) 47 m and d) 85 m. Black dots denote bin-averages of ϵ , where bins contain equal numbers of data points.

conditions (Fig. 5). At 47 m, bin-averaged values of ϵ plotted against $u_*^3/\kappa z$ fall along a 1:1 line (Fig. 5a) and the average value of $\frac{\epsilon \kappa z}{u_*^3}$ is very close to unity (0.96; Table 2). Natural variability in turbulence is estimated to be a factor of 2 (Moum et al. 1995), so scaling of ϵ to within ± 2 of unity can be considered adequate (Miller et al., 2023; Zippel et al., 2021). Binned measurements of ϵ at 47 m show a linear increase with B_0 , though with measurements of ϵ biased high relative to B_0 (Fig. 5b). At 85 m, binned measurements of ϵ also show linear relationships with both $u_*^3/\kappa z$ and B_0 in wind- and buoyancy-dominant conditions, respectively, but the measurements are biased high (Fig. 5 c,d). The average bias in ϵ at 85 m relative to $u_*^3/\kappa z$ is 6.31, but reduces to 3.64 from June–October (Table 2), when the water column is fully destratified (Fig. 4b). In contrast, average bias in ϵ at 47 m remains close to unity year-round.

3.4. Appearance of the salinity signal at DIT

DITN and DITD are located along the northern flank of DIT outside of the primary pathway of katabatic winds. In contrast to the fully-destratified water column observed during austral winter at the LDEO mooring (Figs. 3 and 4b), salinity measurements at DITN (Stevens et al., 2024) suggest that this region of TNB along the northern flank of DIT never fully destratifies; the deepest salinity measurements remain decoupled from the mid-water column and shallow measurements year-round (Fig. 6). However, there is an increase in salinity during September in both the near-seabed salinity time series at DITN and DITD, suggesting HSSW is advected in laterally at depth (Fig. 6). Notably, much of the increase at DITD occurs as a rapid jump over the course of a week, while salinity at DITN increases more gradually, over several weeks. The influx of HSSW at DITD also appears slightly warmer than that at DITN, and both water masses are warmer and saltier on average than the near-bed HSSW at the LDEO mooring in the month prior (Fig. 7). A difference in rolling 10-day-average near-seabed current directions is also seen at DITD and DITN, with currents at the former primarily northward and at the latter, southeastward (Stevens et al., 2024), though with substantial temporal variability. In the month before the September increase in near-seabed salinity, the currents are largely northward and westward (Fig. 6), respectively. Rolling 10-day-average currents near the seafloor at the LDEO mooring site show currents generally in the direction of winds throughout the katabatic wind season (February through October), except at the deepest sensor, where currents veer to the left of the winds (northeastward), away from the direction of DIT.

4. Discussion

Miller et al. 2024 used the LDEO mooring dataset to quantify HSSW production rates in TNB and explore the response of HSSW production to the katabatic wind regime. Here, we build on this work by examining the spatial variability, water column destratification, time scales, and propagation pathways associated with HSSW production.

Table 2

Classic boundary layer scaling (BLS) bias for turbulent kinetic energy dissipation rate (ϵ) measurements at 47 m and 85 m at the LDEO mooring. $u_*^3/\kappa z$ and B_0 are examined in wind-dominant ($|z/L_M| < 0.5$) and buoyancy-dominant ($z/L_M < -3$) conditions, respectively. $u_*^3/\kappa z$ is examined across distinct time periods defined by water column stratification shown in Fig. 4b.

	47 m	85 m
$\epsilon \kappa z / u_*^3$ ($ z/L_M < 0.5$)		
All	0.96 (n = 6384)	6.31 (n = 4496)
Feb–Jun	0.80	7.62
Jun–Oct	1.03	3.64
Oct–Mar	1.09	7.09
ϵ / B_0 ($z/L_M < -3$)	6.81 (n = 185)	30.57 (n = 258)

4.1. Spatial variability in the response of near-surface salinity to winds

The different katabatic wind pathways through the David, Larson, Reeves, and Priestley glaciers (Fig. 1) cause spatial variability in the response of the surface ocean of the TNB Polynya to winds. A tight coupling of the upper ocean to winds at the LDEO mooring site, located along the Nansen Ice Shelf in the direct path of the Reeves Glacier, the dominant katabatic wind pathway in TNB (Bromwich et al., 1990; Ciappa et al. 2012), is demonstrated by the strong correlations between salinity at 47 m with lagged wind speeds at AWS Manuela (Fig. 2a) from April through October, as well as the rapid mixing of brine at the surface to the deepest instrument at 360 m during winter months. This is different from the near-surface response observed at DITN, as well as previous observations at CLIMA Moorings L (Le Bel et al. 2021). At DITN, located in the southeastern corner of TNB along the DIT, salinity measurements at 75 m are uncorrelated with winds at AWS Manuela, and the seasonal increase in salinity at this depth during winter months lags that at the LDEO mooring by roughly a month, never reaching values upward of 34.8 that are typical of HSSW in TNB (Fig. 6). This seasonal increase in upper-ocean salinity may result from advection from the more active sea ice production region along the Nansen Ice Shelf, as speculated by Yoon et al. 2020, or from relatively weak, in-situ sea ice production driven by winds funneled through the Larson or David Glaciers. At CLIMA Mooring L in the northwestern corner of TNB, Le Bel et al. 2021 observed lag times of ~ 5 days between salinity at ~ 30 m depth with winds measured at AWS Rita. This is much longer than the roughly 20 h response lag of near-surface salinity to winds at the LDEO mooring, despite their similar proximity to the front of the ice shelf. Furthermore, it was found that near-surface salinity correlated strongly with wind speed in austral fall but not in austral winter, when polynya-wide sea ice and HSSW production is most active in TNB (Rusciano et al. 2013; Miller et al. 2024). This suggests that, as with DITN, this outer region of the bay experiences less active in-situ ice production and overall looser coupling to winds than the central region where the LDEO mooring is deployed. This is consistent with observations by Ciappa et al. 2012, which found that while the open water area in front of AWS Manuela responded nearly immediately to wind forcing, the open water area in front of AWS Rita and Eneide (near CLIMA Mooring L) lagged by 5 h. Overall, a picture emerges in which HSSW forms primarily in the katabatic-wind-forced region adjacent to the Reeves Glacier portion of the Nansen Ice Shelf (e.g., blue-shaded region in Fig. 8) and circulates to the outer reaches of the bay (Yoon et al. 2020; Mathiot et al. 2012).

4.2. The timing of HSSW production

While salinity increases at the 47 m sensor on the LDEO mooring beginning in mid-March and a strong coupling to winds is observed from April onward (Fig. 3), HSSW production does not begin until later in the winter season. For HSSW to occur, katabatic winds must break down lingering summertime stratification and allow brine produced at the surface to reach pools of HSSW at depth (e.g., Rusciano et al. 2013). This breakdown of stratification is complete at the LDEO mooring by late June (Fig. 3f, Fig. 4b) and is reflected in the jump in correlation between the shallowest and deepest salinity measurements from the April–June period (Fig. 3b) to the June–August period (Fig. 3c). Rusciano et al. 2013 described two phases of polynya function, based on time series from CLIMA Mooring D across 1995–2008: An early-winter period from March through June during which brine rejection works to break down stratification, increasing the salinity at the surface but not resulting in HSSW formation, and a second period from July through October defined by a mixed water column and HSSW production. The initial decrease in salinity seen at each depth at the LDEO mooring across March and April (Fig. 3f) was also observed at CLIMA Mooring D by Rusciano et al. 2013, and is the result of the deepening surface mixed layer entraining and diluting the saltier, stratified waters at depth. This

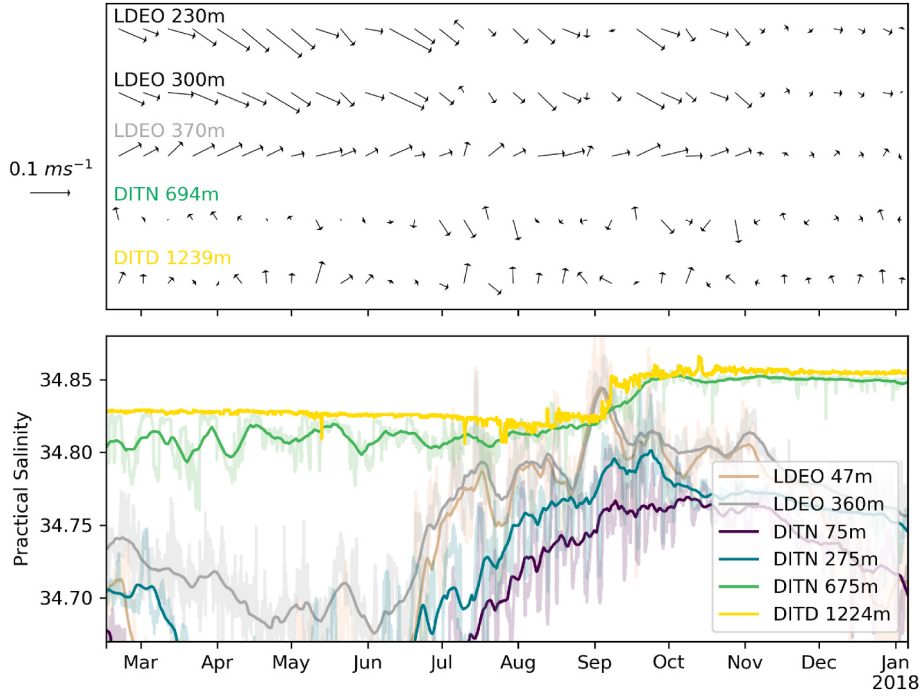


Fig. 6. a) 10-day rolling averages of horizontal current velocities near the seabed at the LDEO, DITN, and DITD moorings. b) 10-day rolling averages of the shallowest and deepest available practical salinity time series at each mooring, illustrating spatial variability in the presence of HSSW as well as the extent to which full-water-column destratification occurs.

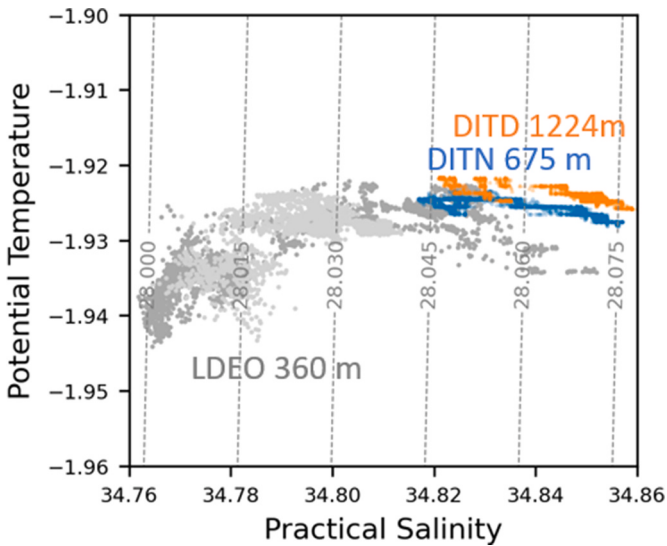


Fig. 7. Near-seabed water masses at the LDEO, DITN, and DITD mooring sites in and preceding the time during which a pulse of High Salinity Shelf Water is seen at the latter two sites. LDEO data shown in light grey are from Aug 1–15 and in dark grey, Aug 15 – Sept 1. DITN and DITD data shown are from Sept 1 – Oct 1.

mechanism was replicated by Le Bel et al. 2021 in 1-dimensional, brine-rejecting mixed layer model runs initialized with CTD-cast data from various locations around TNB. It is notable that though the HSSW production rate (Miller et al. 2024) and salinity (Yoon et al. 2020) in TNB vary year to year, the similarity in timing seen in our 2017 data with that observed 1-2 decades prior suggests that the timing of HSSW production in TNB each year remains relatively consistent.

4.3. The role of turbulence in HSSW production

In-situ measurements of ε are sparse across the world's oceans, and even more so in remote regions such as Antarctic polynyas. Turbulent mixing facilitates HSSW production by breaking down stratification and moving surface brine to depth, and is therefore a key component of HSSW production. To the best of our knowledge, no time series measurements of ε have previously been obtained in a wintertime polynya setting, and we take this opportunity to examine how well classic BLS holds in HSSW-formation conditions.

The scaling of turbulence provides both insight into, as well as a means for the parameterization of, the wind-, wave-, and buoyancy-driven processes that mix momentum, heat, and solutes across the air-sea interface and to depth. Away from the generation and transport of TKE by waves at the surface (e.g. Gerbi et al. 2009; Terray et al. 1996), ocean measurements of ε have been shown by some studies to generally conform to classic BLS: LOW above the depth of L_M and Equation (5) below it (e.g., Lombardo and Gregg, 1989; Esters et al. 2018; Miller et al., 2023). It is important to note that turbulence, by nature, is intermittent in both time and space, thus BLS can only be expected to predict values of ε on average (Zippel et al., 2021; Miller et al., 2023). Most studies of turbulence scaling have been conducted in relatively mild open-ocean conditions, and turbulence scaling in the extreme katabatic wind regime that defines the polynya system (e.g., Guest, 2021b; Guest 2021a; Wenta and Cassano 2020) remains unknown.

Belcher et al., (2012) made a scaling-based argument that Langmuir circulation plays an important role in surface ocean turbulent mixing and the deepening of mixed layers, particularly in the open Southern Ocean. It has been proposed that biases in mixed layer depths produced by models are due to their reliance on classic BLS, which does not incorporate Langmuir circulation, to parameterize sub-grid turbulent fluxes in the ocean boundary layer. As field measurements of surface fluxes and ε are sparse, especially in the polar regions, this remains an open question. Ferris et al., (2022) observed gilder-based measurements of ε to deviate from classic BLS within the strongly wind-forced setting of the Antarctic Circumpolar Current, but attributed discrepancies at depth

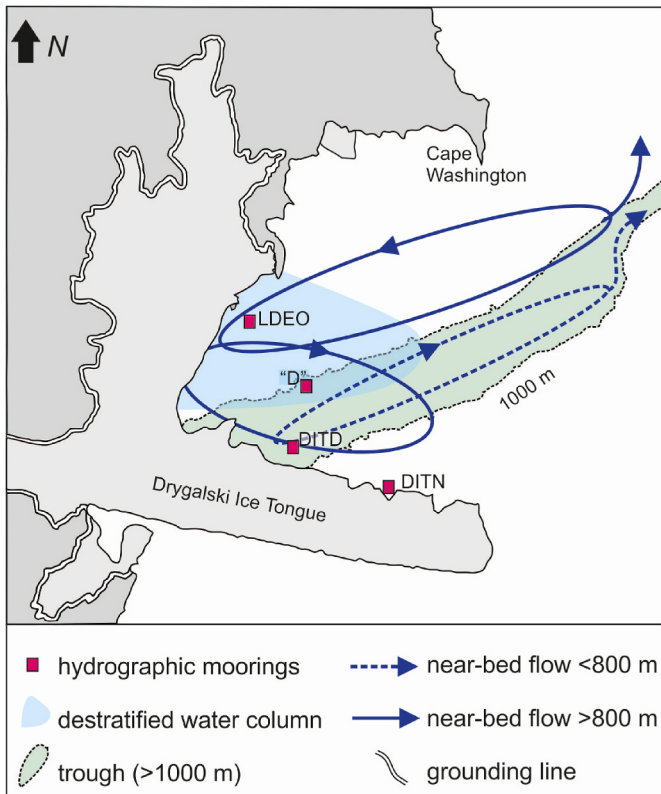


Fig. 8. A possible wintertime circulation scheme that could explain the near-seabed HSSW signals observed at LDEO, DITN, and DITD, loosely based on circulation schemes proposed by Xu et al. (2023b) and Yoon et al. (2020) and consistent with velocity measurements at the three mooring sites in the month prior to the appearance of the HSSW signal along DIT. Only the 1000 m isobath is shown for visual simplicity. Note that all features, including the blue-shaded region indicating a destratified water column, would change in size and extent depending on the katabatic wind regime.

only partially to the generation and redistribution of TKE by Langmuir Circulation; instead, shear associated with storm-generated near-inertial currents, double diffusion, and other turbulent processes were proposed to play a significant role, and it was still determined that classic BLS outperformed other, wave-based BLS. That our measurements of ε at 47 m, and to some degree, at 85 m, scale with $u_*^3/\kappa z$ is perhaps surprising, as Langmuir circulation occurs regularly in the TNB Polynya, where wind-aligned streaks of frazil ice are regularly observed across the open area of the polynya in satellite imagery such that they are reliably used to define polynya extent (Ciappa and Pietranera 2013). However, measurements of ε scaling according to classic BLS does not mean that Langmuir turbulence has no contribution to mixed layer turbulence within the polynya, but rather that it may scale to wind-driven current shear turbulence in a way that it is implicitly captured by $u_*^3/\kappa z$, as suggested by Miller et al., (2023).

The year-round underestimation of ε by $u_*^3/\kappa z$ at 85 m may be indicative of other turbulent processes not considered in classic BLS. We rule out the influence of Langmuir circulation, as that would induce biases at both instruments. That the bias is seen to a higher degree in the deeper instrument suggests there may be a source of TKE from deeper in the water column, such as the breaking of internal waves formed at the bottom boundary of the mixed layer. The possible influence of internal wave activity at the bottom of the mixed layer is supported by the decreased bias observed at 85 m from June through October, when the water column is fully destratified, relative to periods during which the water column is actively de-stratifying and re-stratifying (Table 2), which would situate the bottom boundary of the mixed layer nearer to

the 85 m instrument. Internal waves are likely a prominent feature in TNB, as summer surface heating and glacial melt creates strong vertical density gradients in the water column at which internal waves can form. Tidal flow (Wang et al., 2013; Bowen et al. 2023) over bathymetric features (Laurent et al., 2012), including the slope leading up to the Nansen Ice Shelf, as well rapid changes in wind forcing (e.g., the periodic rise and fall of katabatic winds), are plausible mechanisms by which internal waves would regularly form in TNB. That ε remains elevated at 85 m relative to LOW with a bias of 3.64 (Table 2) in the absence of strong vertical density gradients at the mooring site suggests that internal waves at the bottom of the mixed layer would not constitute the full story, however. In a dynamic coastal environment such as TNB, there are many 3-dimensional processes that are beyond the view of a 1-dimensional mooring that could, in addition internal waves, enhance TKE at depth. We also note that measurements at the 85 m instrument exhibited, on average, lower correlations (a measure of pulse-pair quality) as well as fitted noise estimates as high as order magnitude 10^{-6} . While low-correlation measurements are removed via a correlation threshold and instrument noise is accounted for in the spectral fit (Equation (2)), this suggests that data from this lower instrument may be of lower reliability than those at 47 m.

Measurements of ε in buoyancy-dominant (i.e., low-wind) conditions scale with B_0 but are systematically biased high at both instrument depths (Fig. 4, Table 2). This may be because convective turbulence is weaker relative to wind-forced turbulence, and therefore instrument noise and other turbulence processes not accounted for by classic BLS are more pronounced in the relatively low-turbulence setting of buoyancy-dominant conditions (Ferris et al., 2022).

While our measurements of ε do not all strictly conform to the magnitudes predicted by classic BLS, they do generally scale with $u_*^3/\kappa z$ and B_0 , and in the case of measurements at 47 m in wind-dominating conditions, scale 1:1 according to LOW. We can assess the applicability of classic BLS to the polynya environment in the context of timescales for the mixing of brine at the surface to depth, or, the production of HSSW. Thompson et al. 2020 presented a timescale, t , for turbulence to mix away salinity anomalies caused by brine rejection, based on an eddy turnover time,

$$t = (L_M^2 \varepsilon)^{1/3} \quad (7)$$

where L_M represents the length scale of the largest wind-driven eddy. We adapt this timescale to represent the time that wind-driven shear turbulence takes to mix brine at the surface to the bottom of the water column. If we take ε from the 47 m instrument across April through September to be representative of an average across the full water column at the LDEO mooring site (values will be several orders of magnitude higher at the surface and lower at depth), Equation (7) yields an average of approximately 2.5 h, with a standard deviation of 2 h. This is consistent with our correlation analysis of salinity at 47 m with that at 360 m, which shows the surface salinity signal propagates to depth in about 5 h or less over the same time period (Fig. 2b). While this is a loose approximation, it suggests that classic BLS could have some utility in a polynya setting, where wind-driven turbulent mixing plays a direct role in HSSW formation.

4.4. Pathways for HSSW transport within TNB

HSSW is present at depth throughout TNB, but evidence for in-situ formation is only found in a strongly wind-forced and well-mixed region extending from the Nansen Ice Shelf front, in the path of katabatic wind channeled through the Reeves Glacier (Yoon et al. 2020; Miller et al. 2024). Thus, HSSW observed at the near-seabed of DITD and DITN is likely advected from this shelf-front formation region over the course of the HSSW production season. Based on the observed differences in the water mass properties, current velocities, and timing of the September HSSW signal at the two mooring sites, it appears that HSSW travels

along two separate pathways to reach DIT (Yoon et al. 2020).

What near-seabed pathways could feasibly connect the HSSW formed and observed at the LDEO mooring with HSSW observed at DITN and DITD? One possibility, as Yoon et al. 2020 speculated, is the bay-wide clockwise circulation pattern previously observed in satellite imagery by van Woert et al. (2001), coupled with a clockwise circulation pattern contained within the Drygalski Basin. Both of these patterns were substantiated by summertime lowered-ADCP (LADCP) measurements throughout the bay. The study noted, however, that these patterns have not been observed to occur outside of summer months and do not necessarily persist year-round. Indeed, recent model simulations of TNB suggest that more complex circulation schemes emerge under winter conditions: A climatology-and-reanalysis forced simulation of TNB recreated the bay-wide clockwise pattern as well as the clockwise Drygalski pattern observed during summer months, but produced a smaller-scale, eddying pattern during winter months at 600 m depth across the Bay and within the Drygalski Basin (Kim et al., 2023). While the ERA5 product used for wind-forcing in Kim et al., 2023 does not capture katabatic winds, these findings support significant seasonal differences in circulation in TNB. Xu et al. (2023b) ran model simulations in an idealized TNB-like polynya environment with explicit katabatic wind forcing that produced a counterclockwise vortex in the northern half of the modeled TNB at the surface and bottom of the water column, and a second, smaller clockwise vortex in the southern half at the bottom. These vortices spread HSSW formed along Nansen Ice Shelf front to the outer reaches of the bay and beyond (e.g., Fig. 6f of Xu et al., 2023b). A similar dipole structure at the surface was proposed by Friedrichs et al. 2022 based on summertime visible satellite imagery following a period of strong winds.

Based on the simulation presented in Xu et al. (2023b), we propose a possible circulation scheme that is consistent with the near-seabed velocities observed at LDEO, DITD, and DITN in the month prior to the HSSW pulse seen at the latter two moorings in September (Fig. 8). Here, HSSW formed around the LDEO mooring is entrained into two counter-rotating vortices that form in response to katabatic winds. Some of the HSSW entrained in the clockwise vortex is advected to DITN, while some of it is further entrained into the clockwise Drygalski Basin circulation pattern described by Yoon et al. (2020). That the observed HSSW arriving to DITN and DITD in September is on average warmer and saltier than that formed at the LDEO mooring in the month prior (Fig. 7) is consistent with a circuitous path for HSSW formed along the Nansen Ice Shelf that results in mixing with warmer and saltier ambient water masses in the bay, including previous years' HSSW. While Fig. 8 represents one possible circulation pattern for HSSW, near-seabed currents (Fig. 6) suggest variability in the extent and even direction of these circulation patterns across the winter season. Data from DITN, in particular, hint at such complexity: near-seabed currents at DITN are largely westward in the month prior to appearance of HSSW in September, but are often southward and southeastward throughout the year. Stevens et al., 2024 found similar hydrographic properties between DITN and a concurrent mooring on the southern side of DIT, which, combined with current velocity measurements, suggest that for part of the year at DITN, there is flow of HSSW exiting TNB rather than recirculating within it. A clearer picture of circulation of HSSW in the bay will emerge as more wintertime moored observations are made in TNB, allowing for a greater understanding of how variability in this key water mass can propagate to AABW downstream.

5. Summary

Here, we have used data from a densely-instrumented upper-ocean mooring in a region of active HSSW formation within TNB to explore key aspects of HSSW formation and transport. We find brine rejection to be tightly coupled to katabatic winds at the LDEO mooring site, with high correlations ($R > 0.6$) between near-surface salinity and time-lagged (-20 h) wind speeds at AWS Manuela for much of the active HSSW

production season from June through October. During this period, turbulent mixing is strong, with elevated measurements of ϵ at 47 and 85 m on the order of 10^{-6} W kg⁻¹ and a surface-to-depth salinity signal propagation of only 5 h. The turbulence regime is strongly wind-driven, and measurements of ϵ show some agreement with classic BLS, especially bin-averaged ϵ at 47 m, which scales 1:1 with values predicted according to LOW. Data from moorings along the northern flank of the DIT and previously published studies of CLIMA Moorings D and L suggest that the outer periphery of TNB is at most weakly coupled to the katabatic wind regime and thus does not contribute significantly to HSSW production. Rather, HSSW production is centered in the path of katabatic winds from the Reeves Glacier (Fig. 8), which encompasses the LDEO mooring and CLIMA Mooring D. We review current knowledge of the circulation pathways for HSSW within TNB (Yoon et al. 2020; Xu et al. 2023b; Xu et al. 2023a; Kim et al., 2023) and propose a near-seabed circulation pattern for HSSW that is consistent with model studies and our analysis of moored observations (Fig. 8). While such polynya processes and dynamics are relatively small in scale, their impact on HSSW production and downstream AABW extend the reach of their significance far beyond the boundaries of TNB.

Data availability

The LDEO mooring data, including temperature, salinity, and turbulent kinetic energy (TKE) dissipation rates, are available from <https://doi.org/10.7916/a4k3-0a14>. Velocity, correlation, amplitude, and other outputs from the 2 MHz Nortek AquaDopp High-Resolution Pulse-Coherent ADCPs used to estimate TKE dissipation rates are available from <https://doi.org/10.7916/c0j2-0w55>. AWS Manuela data are available from <https://amrc.ssec.wisc.edu/aws/>.

CRediT authorship contribution statement

Una Kim Miller: Writing – original draft, Visualization, Validation, Software, Formal analysis, Data curation. **Christopher J. Zappa:** Writing – review & editing, Project administration, Funding acquisition, Formal analysis, Conceptualization. **Arnold L. Gordon:** Writing – review & editing, Funding acquisition, Formal analysis, Conceptualization. **Seung-Tae Yoon:** Writing – review & editing, Formal analysis. **Craig Stevens:** Writing – review & editing, Formal analysis, Data curation. **Liv Cornelissen:** Writing – review & editing, Data curation. **Sukyoung Yun:** Writing – review & editing, Data curation. **Won Sang Lee:** Writing – review & editing, Resources.

Declaration of competing interest

The authors declare that they have no known competing financial interests or personal relationships that could have appeared to influence the work reported in this paper.

Acknowledgements

We thank two anonymous reviewers for their insightful comments as well as the scientists and ship crew involved in cruises ANA07C and ANA08C aboard the R/V Araon. The deployment and recovery of the LDEO mooring was made possible with support from National Science Foundation (NSF) grant PLR 13-41688, with additional support for C.Z. and A.G. from NSF Office of Polar Programs (OPP) award 2332418. U.K. M was supported by National Aeronautics and Space Administration (NASA) award 80NSSC19K1348. S-TY was supported by the NRF grant funded by Ministry of Education (2022R1I1A3063629). S-TY, W.S.L, and S.Y. were supported by the Korea Institute of Marine Science & Technology Promotion (KIMST) funded by the Ministry of Oceans and Fisheries(RS-2023-00256677; PM24020). C.S. and L.C. were supported by the New Zealand Antarctic Science Platform (ANTA1801). The AWS Manuela dataset is made available courtesy of the Wisconsin-Madison

Automatic Weather Station Program, funded by NSF grant 1924730. We also wish to acknowledge the Norwegian Polar Institute's Quantarctica package and the General Bathymetric Chart of the Ocean (GEBCO) Compilation Group.

References

- Ackley, S.F., Stammerjohn, S., Maksym, T., Smith, M., Cassano, J., Guest, P., Tison, J.-L., Delille, B., Loose, B., Sedwick, P., DePace, L., Roach, L., Parno, J., 2020. "Sea-ice production and air/ice/ocean/biogeochemistry interactions in the Ross Sea during the PIPERS 2017 autumn field campaign". en *Ann. Glaciol.* 61 (82), 181–195. <https://doi.org/10.1017/aog.2020.31>. Publisher: Cambridge University Press issn: 0260-3055, 1727-5644.
- Alucino, Giuseppe, Sansiviero, Manuela, Paul, Stephan, Cesaran, Cinzia, Fusco, Giannetta, Wadhams, Peter, Budillon, Giorgio, 2018. "A new approach for monitoring the Terra Nova bay polynya through MODIS ice surface temperature imagery and its validation during 2010 and 2011 winter seasons". en *Rem. Sens.* 10 (3), 366. <https://doi.org/10.3390/rs10030366>.
- Belcher, Stephen E., Grant, Alan L.M., Hanley, Kirsty E., Fox-Kemper, Baylor, Van Roekel, Luke, Sullivan, Peter P., Large, William G., Brown, Andy, Hines, Adrian, Calvert, Daley, Rutgersson, Anna, Pettersson, Heidi, Bidlot, Jean-Raymond, Janssen, Peter A.E. M., Polton, Jeff A., 2012. "A global perspective on Langmuir turbulence in the ocean surface boundary layer". en *Geophys. Res. Lett.* 39 (18). <https://doi.org/10.1029/2012GL052932>.
- Bowen, Melissa M., Fernandez, Denise, Gordon, Arnold L., Huber, Bruce, Castagno, Pasquale, Falco, Pierpaolo, Budillon, Giorgio, Gunn, Kathryn L., Forcen-Vazquez, Aitana, 2023. Tides regulate the flow and density of antarctic bottom water from the western Ross Sea. en *Sci. Rep.* 13 (1), 3873. <https://doi.org/10.1038/s41598-023-31008-w>. Number: 1 Publisher: Nature Publishing Group issn: 2045-2322.
- Bromwich, David H., Kurtz, Dennis D., 1982. Experiences of Scott's Northern Party: evidence for a relationship between winter katabatic winds and the Terra Nova Bay polynya. en *Polar Rec.* 21 (131), 137–146. <https://doi.org/10.1017/S0032247400004514>. Publisher: Cambridge University Press issn: 1475-3057, 0032-2474.
- Bromwich, David H., Parish, Thomas R., Zorman, Christian A., 1990. "The confluence zone of the intense katabatic winds at Terra Nova Bay, Antarctica, as derived from airborne sastrugi surveys and mesoscale numerical modeling". en *J. Geophys. Res. Atmos.* 95 (D5), 5495–5509. <https://doi.org/10.1029/JD095iD05p05495>. issn: 2156-2202_eprint.
- Bromwich, David H., 1989. Satellite analyses of antarctic katabatic wind behavior. *Bull. Am. Meteorol. Soc.* 70 (7), 738–749. [https://doi.org/10.1175/1520-0477\(1989\)070<0738:SAOAKW>2.0.CO;2](https://doi.org/10.1175/1520-0477(1989)070<0738:SAOAKW>2.0.CO;2) issn: 0003-0007.
- Budillon, Giorgio, Fusco, Giannetta, Spezie, Giancarlo, 2000. "A study of surface heat fluxes in the Ross Sea (Antarctica)". en *Antarct. Sci.* 12 (2), 243–254. <https://doi.org/10.1017/S0954102000000298>. Publisher: Cambridge University Press issn: 1365-2079, 0954-1020.
- Castagno, Pasquale, Capozzi, Vincenzo, DiTullio, Giacomo R., Falco, Pierpaolo, Fusco, Giannetta, Rintoul, Stephen R., Spezie, Giancarlo, Budillon, Giorgio, 2019. "Rebound of shelf water salinity in the Ross Sea". en *Nat. Commun.* 10 (1), 5441. <https://doi.org/10.1038/s41467-019-13083-8>. Number: 1 Publisher: Nature Publishing Group issn: 2041-1723.
- Ciappa, Achille, Pietranera, Luca, 2012. The Terra Nova Bay (Antarctica) polynya observed by MODIS ice surface temperature imagery from May to June 2009. *Int. J. Rem. Sens.* 33 (14), 4567–4582. <https://doi.org/10.1080/01431161.2011.652314> issn: 0143-1161.
- Ciappa, Achille, Pietranera, Luca, 2013. High resolution observations of the Terra Nova Bay polynya using COSMO-SkyMed X-SAR and other satellite imagery. *J. Mar. Syst.* 113–114, 42–51. <https://doi.org/10.1016/j.jmarsys.2012.12.004> issn: 0924-7963.
- Ciappa, Achille, Pietranera, Luca, Budillon, Giorgio, 2012. Observations of the Terra Nova Bay (Antarctica) polynya by MODIS ice surface temperature imagery from 2005 to 2010. *Rem. Sens. Environ.* 119, 158–172. <https://doi.org/10.1016/j.rse.2011.12.017> issn: 0034-4257.
- Esters, L., Breivik, Ø., Landwehr, S., ten Doeschate, A., Sutherland, G., Christensen, K.H., Bidlot, J.-R., Ward, B., 2018. "Turbulence scaling comparisons in the Ocean surface boundary layer". en *J. Geophys. Res.: Oceans* 123 (3), 2172–2191. <https://doi.org/10.1002/2017JC013525>. issn: 2169-9291.
- Fairall, C.W., Bradley, E.F., Rogers, D.P., Edson, J.B., Young, G.S., 1996. "Bulk parameterization of air-sea fluxes for tropical ocean-global atmosphere coupled-ocean atmosphere response experiment". en *J. Geophys. Res.: Oceans* 101 (C2), 3747–3764. <https://doi.org/10.1029/95JC03205>. issn: 2156-2202_eprint.
- Fairall, C.W., Bradley, E.F., Hare, J.E., Grachev, A.A., Edson, J.B., 2003. "Bulk parameterization of air-sea fluxes: updates and verification for the COARE algorithm". en *J. Clim.* 16 (4), 571–591. [https://doi.org/10.1175/1520-0442\(2003\)016<0571:BPOASF>2.0.CO;2](https://doi.org/10.1175/1520-0442(2003)016<0571:BPOASF>2.0.CO;2). Publisher: American Meteorological Society Section: Journal of Climate issn: 0894-8755, 1520-0442.
- Ferris, Laur, Gong, Donglai, Anne Clayton, Carol, Merrifield, Sophia, Shroyer, Emily L., Smith, Madison, Laurent, Louis St, 2022. "Shear turbulence in the high-wind southern ocean using direct measurements". en *J. Phys. Oceanogr.* 52 (10), 2325–2341. <https://doi.org/10.1175/JPO-D-21-0015.1>. Publisher: American Meteorological Society Section: Journal of Physical Oceanography issn: 0022-3670, 1520-0485.
- Friedrichs, Drew M., McInerney, Jasmin B.T., Oldroyd, Holly J., Lee, Won Sang, Yun, Sukyoung, Yoon, Seung-Tae, Stevens, Craig L., Zappa, Christopher J.,
- Dow, Christine F., Mueller, Derek, Steiner, Oscar Sepúlveda, Forrest, Alexander L., 2022. "Observations of submesoscale eddy-driven heat transport at an ice shelf calving front". en *Communications Earth & Environment* 3.1, 1–9. <https://doi.org/10.1038/s43247-022-00460-3>. Number: 1 Publisher: Nature Publishing Group issn: 2662-4435.
- Fusco, Giannetta, Budillon, Giorgio, Spezie, Giancarlo, 2009. "Surface heat fluxes and thermohaline variability in the Ross Sea and in Terra Nova bay polynya". en *Continent. Shelf Res.* 29 (15), 1887–1895. <https://doi.org/10.1016/j.csr.2009.07.006>. issn: 0278-4343.
- Gerbi, Gregory P., Trowbridge, John H., Terray, Eugene A., Plueddemann, Albert J., Kukulka, Tobias, 2009. "Observations of turbulence in the Ocean surface boundary layer: energetics and transport". en *J. Phys. Oceanogr.* 39 (5), 1077–1096. <https://doi.org/10.1175/2008JPO4044.1>. Publisher: American Meteorological Society Section: Journal of Physical Oceanography issn: 0022-3670, 1520-0485.
- Gordon, Arnold L., 1970. Vertical momentum flux accomplished by Langmuir circulation. en *J. Geophys. Res.* 4177–4179. <https://doi.org/10.1029/JC075i021p04177> (1896–1977) issn: 2156-2202 75.21. _eprint.
- Gordon, Arnold L., Zambianchi, Enrico, Orsi, Alejandro, Visbeck, Martin, Giulivi, Claudia F., Whitworth, Thomas, Spezie, Giancarlo, 2004. "Energetic plumes over the western Ross Sea continental slope". en *Geophys. Res. Lett.* 31, 21. <https://doi.org/10.1029/2004GL020785>. _eprint.
- Gordon, Arnold L., Huber, Bruce A., Busecke, Julius, 2015. "Bottom water export from the western Ross Sea, 2007 through 2010". en *Geophys. Res. Lett.* 42.13, 5387–5394. <https://doi.org/10.1002/2015GL064457>. issn: 1944-8007_eprint.
- Gordon, Arnold L., Orsi, Alejandro H., Muench, Robin, Huber, Bruce A., Zambianchi, Enrico, Visbeck, Martin, 2009. Western Ross Sea continental slope gravity currents. *Deep-Sea Res. Part II: Topical Studies in Oceanography*. Southern Ocean Shelf Slope Exchange 56 (13), 796–817. <https://doi.org/10.1016/j.dsr.2008.10.037> issn: 0967-0645.
- Guest, P.S., 2021b. "Inside katabatic winds over the Terra Nova bay polynya: 2. Dynamic and thermodynamic analyses". en *J. Geophys. Res. Atmos.* 126.20. <https://doi.org/10.1029/2021JD034904>. _eprint. <https://agupubs.onlinelibrary.wiley.com/doi/pdf/10.1029/2021JD034904.e2021JD034904.issn:2169-8996>.
- Guest, P.S., 2021a. "Inside katabatic winds over the Terra Nova bay polynya: 1. Atmospheric jet and surface conditions". en *J. Geophys. Res. Atmos.* 126 (20). <https://doi.org/10.1029/2021JD034902>. Publisher: John Wiley & Sons, Ltd, e2021JD034902. issn: 2169-8996.
- Jacobs, S.S., Giulivi, C.F., Dutrieux, P., 2022. "Persistent Ross Sea freshening from imbalance west antarctic ice shelf melting". en *J. Geophys. Res.: Oceans* 127 (3). <https://doi.org/10.1029/2021JC017808>. _eprint.
- Jenderski, Stefan, Williams, Michael J.M., Langhorne, Pat J., Robertson, Robin, 2018. "The density-driven winter intensification of the Ross Sea circulation". en *J. Geophys. Res.: Oceans* 123 (11), 7702–7724. <https://doi.org/10.1029/2018JC013965>. issn: 2169-9291_eprint.
- Kim, Taekyun, Hong, Ji-Seok, Jin, Emilia Kyung, Moon, Jae-Hong, Song, Sang-Keun, Lee, Won Sang, 2023. Spatiotemporal variability in ocean-driven basal melting of cold-water cavity ice shelf in Terra Nova Bay, East Antarctica: roles of tide and cavity geometry. *English Front. Mar. Sci.* 10, 2296–7745. <https://doi.org/10.3389/fmars.2023.1249562>. Publisher: Frontiers. issn.
- Kolmogorov, A., 1941. *The local structure of turbulence in incompressible viscous fluid for very large Reynolds' numbers*. *Akademiia Nauk SSSR Doklady* 30, 301–305 issn: 0002-3264.
- Laurent, L., St. Naveira Garabato, A.C., Ledwell, J.R., Thurnherr, A.M., Toole, J.M., Watson, A.J., 2012. Turbulence and diapycnal mixing in drake passage. EN. In: *J. Phys. Oceanograph.* 42 (12), 2143–2152. <https://doi.org/10.1175/JPO-D-12-027.1>. Publisher: American Meteorological Society Section: Journal of Physical Oceanography. issn: 0022-3670, 1520-0485.
- Le Bel, Deborah A., Zappa, Christopher J., Budillon, Giorgio, Gordon, Arnold L., 2021. "Salinity response to atmospheric forcing of the Terra Nova Bay polynya, Antarctica". en *Antarct. Sci.* 33 (3), 318–331. <https://doi.org/10.1017/S0954102021000146>. Publisher: Cambridge University Press issn: 0954-1020, 1365-2079.
- Lombardo, C.P., Gregg, M.C., 1989. "Similarity scaling of viscous and thermal dissipation in a convecting surface boundary layer". en *J. Geophys. Res.: Oceans* 94 (C5), 6273–6284. <https://doi.org/10.1029/JC094iC05p06273>. issn: 2156-2202_eprint.
- Martin, Seeleye, Drucker, Robert S., Kwok, Ronald, 2007. "The areas and ice production of the western and central Ross Sea polynyas, 1992–2002, and their relation to the B-15 and C-19 iceberg events of 2000 and 2002". *J. Mar. Syst.* 68 (1), 201–214. <https://doi.org/10.1016/j.jmarsys.2006.11.008> issn: 0924-7963.
- Mathiou, Pierre, Jourdain, Nicolas C., Barnier, Bernard, Gallée, Hubert, Molines, Jean Marc, Sommer, Julien Le, Penduff, Thierry, 2012. "Sensitivity of coastal polynyas and high-salinity shelf water production in the Ross Sea, Antarctica, to the atmospheric forcing". en *Ocean Dynam.* 62 (5), 701–723. <https://doi.org/10.1007/s10236-012-0531-y> issn: 1616-7228.
- Matsuoka, Kenichi, Skoglund, Anders, Roth, George, de Pomereu, Jean, Griffiths, Huw, Headland, Robert, Herried, Brad, Katsumata, Katsuro, Le Brocq, Anne, Licht, Kathy, Morgan, Fraser, Neff, Peter D., Ritz, Catherine, Scheinert, Mirko, Tamura, Takeshi, Putte, Anton Van de, Broeke, Michiel van den, Deschwanden, Angela von, Deschamps-Berger, César, Liefferinge, Brice Van, Tronstad, Stein, Melvær, Yngve, 2021. Quantarctica, an integrated mapping environment for Antarctica, the Southern Ocean, and sub-Antarctic islands. *Environ. Model. Software* 140, 105015. <https://doi.org/10.1016/j.envsoft.2021.105015> issn: 1364-8152.
- McDougall, Trevor J., Barker, Paul M., 2011. *Getting Started with TEOS-10 and the Gibbs Seawater (GSW) Oceanographic Toolbox: Version 3.0*. CSIRO Marine and Atmospheric Research, Hobart, Tas isbn: 978-0-646-55621-5.

- Miller, Una Kim, Zappa, Christopher J., Zippel, Seth F., Thomas Farrar, J., Weller, Robert A., 2023. "Scaling of moored surface ocean turbulence measurements in the southeast pacific ocean". *J. Geophys. Res.: Oceans* 128, 1. <https://doi.org/10.1029/2022JC018901> issn:2169-9291_eprint.
- Miller, Una Kim, Zappa, Christopher J., Gordon, Arnold L., Yoon, Seung-Tae, Stevens, Craig, Lee, Won Sang, 2024. "High salinity shelf water production rates in Terra Nova bay, Ross Sea from high-resolution salinity observations". en *Nat. Commun.* 15, 1, 373. <https://doi.org/10.1038/s41467-023-43880-1>. Number: 1 Publisher: Nature Publishing Group issn: 2041-1723.
- Moum, J.N., Gregg, M.C., Lien, R.C., Carr, M.E., 1995. Comparison of turbulence kinetic energy dissipation rate estimates from two ocean microstructure profilers. en *J. Atmos. Ocean. Technol.* 12 (2), 346–366. [https://doi.org/10.1175/1520-0426\(1995\)012<0346:COTKED>2.0.CO;2](https://doi.org/10.1175/1520-0426(1995)012<0346:COTKED>2.0.CO;2). Publisher: American Meteorological Society Section: Journal of Atmospheric and Oceanic Technology issn: 0739-0572, 1520-0426.
- Orsi, Alejandro H., Wiederwohl, Christina L., 2009. "A recount of Ross Sea waters". *Deep-Sea Res. Part II: Topical Studies in Oceanography*. Southern Ocean Shelf Slope Exchange 56 (13), 778–795. <https://doi.org/10.1016/j.dsr2.2008.10.033> issn: 0967-0645.
- Parmiggiani, Flavio, 2006. Fluctuations of Terra Nova Bay polynya as observed by active (ASAR) and passive (AMSR-E) microwave radiometers. *Int. J. Rem. Sens.* 27 (12), 2459–2467. <https://doi.org/10.1080/01431160600554355> issn: 0143-1161.
- Parkey, Sarah G., Johnson, Gregory C., 2012. Global contraction of antarctic bottom water between the 1980s and 2000s. en *J. Clim.* 25 (17), 5830–5844. <https://doi.org/10.1175/JCLI-D-11-00612.1>. Publisher: American Meteorological Society Section: Journal of Climate issn: 0894-8755 1520-0442.
- Parkey, Sarah G., Johnson, Gregory C., Talley, Lynne D., Sloyan, Bernadette M., Wijffels, Susan E., Smethie, William, Mecking, Sabine, Katsumata, Katsuro, 2019. "Unabated bottom water warming and freshening in the south pacific ocean". en *J. Geophys. Res.: Oceans* 124 (3), 1778–1794. <https://doi.org/10.1029/2018JC014775>, issn: 2169-9291_eprint.
- Rhee, Tae, Zappa, Christopher, Kwon, Young, 2022. Significant Atmospheric CO₂ Uptake by Antarctic Polynyas. <https://doi.org/10.21203/rs.3.rs-1662382/v1>.
- Ruscianno, Emanuela, Budillon, Giorgio, Fusco, Giannetta, Spezie, Giancarlo, 2013. "Evidence of atmosphere-sea ice-ocean coupling in the Terra Nova Bay polynya (Ross Sea—Antarctica)". en *Continent. Shelf Res.* 61–62, 112–124. <https://doi.org/10.1016/j.csr.2013.04.002>, issn: 0278-4343.
- Silvano, Alessandro, Annie, Foppert, Rintoul, Stephen R., Holland, Paul R., Tamura, Takeshi, Kimura, Noriaki, Pasquale, Castagno, Pierpaolo, Falco, Giorgio, Budillon, Alexander, Haumann F., Alberto C., Naveira Garabato, Macdonald, Alison M., 2020. Recent recovery of antarctic bottom water formation in the Ross Sea driven by climate anomalies. *English Nat. Geosci.* 13 (12), 780–786. <https://doi.org/10.1038/s41561-020-00655-3>. Place: London, United States Publisher: Nature Publishing Group issn: 17520894, pp. 780–786.
- Spezie, Giancarlo, Manzella, Giuseppe M.R. (Eds.), 1999. *Oceanography of the Ross Sea, Antarctica*. Medium: Electronic Resource Meeting Name: International Conference on the Oceanography of the Ross Sea. Milan. Springer, New York issn: 978-88-470-0039-1.
- Sreenivasan, Katepalli R., 1995. On the universality of the Kolmogorov constant. *Phys. Fluids* 7 (11), 2778–2784. <https://doi.org/10.1063/1.868656>. Publisher: American Institute of Physics issn: 1070-6631.
- Stevens, C., Yoon, S.T., Zappa, C.J., Miller, U.K., Wang, X., Elliott, F., Cornelissen, L., Lee, C.K., Yun, S., Lee, W.S., 2024. Ocean processes south of the Drygalski Ice Tongue, western Ross Sea. In: *Deep Sea Res. Part II Topical Stud. Oceanograph.* 217, 105411 <https://doi.org/10.1016/j.dsr2.2024.105411> issn: 0967-0645.
- Terray, E.a., Donelan, M.a., Agrawal, Y.c., Drennan, W.m., Kahma, K.k., Williams, A.j., Hwang, P.a., Kitajgorodskii, S.a., 1996. Estimates of kinetic energy dissipation under breaking waves. *J. Phys. Oceanogr.* 26 (5), 792–807. [https://doi.org/10.1175/1520-0485\(1996\)026<0792:EOKEDU>2.0.CO;2](https://doi.org/10.1175/1520-0485(1996)026<0792:EOKEDU>2.0.CO;2) issn: 0022-3670.
- Thompson, Lisa, Smith, Madison, Thomson, Jim, Stammerjohn, Sharon, Ackley, Steve, Loose, Brice, 2020. "Frazil ice growth and production during katabatic wind events in the Ross Sea, Antarctica". *English Cryosphere* 14 (10), 3329–3347. Publisher: Copernicus GmbH issn: 1994-0416.
- van Woert, Michael, L., Meier, Walter N., Zou, Cheng-Zhi, Archer, Andy, Pellegrini, Andrea, Grigioni, Paolo, Bertoia, Cheryl, 2001. "Satellite observations of upper-ocean currents in Terra Nova bay, Antarctica". en *Ann. Glaciol.* 33, 407–412. <https://doi.org/10.3189/172756401781818879>. Publisher: Cambridge University Press issn: 0260-3055, 1727-5644.
- Wang, Q., Danilov, S., Hellmer, H., Sidorenko, D., Schröter, J., Jung, T., 2013. "Enhanced cross-shelf exchange by tides in the western Ross Sea". en *Geophys. Res. Lett.* 40 (21), 5735–5739. <https://doi.org/10.1002/2013GL058207>, issn: 1944-8007_eprint.
- Wenta, Marta, Cassano, John J., 2020. "The atmospheric boundary layer and surface conditions during katabatic wind events over the Terra Nova bay polynya". en *Rem. Sens.* 12 (24), 4160. <https://doi.org/10.3390/rs12244160>. Number: 24 Publisher: Multidisciplinary Digital Publishing Institute issn: 2072-4292.
- Xu, Yilang, Zhang, Weifeng Gordon, Maksym, Ted, Ji, Rubao, Li, Yun, 2023a. "Stratification breakdown in antarctic coastal polynyas. Part I: influence of physical factors on the destratification time scale". en *J. Phys. Oceanogr.* 53 (9), 2047–2067. <https://doi.org/10.1175/JPO-D-22-0218.1>. Publisher: American Meteorological Society Section: Journal of Physical Oceanography issn: 0022-3670, 1520-0485.
- Xu, Yilang, Zhang, Weifeng Gordon, Maksym, Ted, Ji, Rubao, Li, Yun, 2023b. "Stratification breakdown in antarctic coastal polynyas. Part II: influence of an ice Tongue and coastline geometry". en *J. Phys. Oceanogr.* 53 (9), 2069–2088. <https://doi.org/10.1175/JPO-D-22-0219.1>. Publisher: American Meteorological Society Section: Journal of Physical Oceanography issn: 0022-3670 1520-0485.
- Zippel, Seth F., Thomas Farrar, J., Zappa, Christopher J., Miller, Una, St Laurent, Louis, Ijichi, Takashi, Weller, Robert A., McRaven, Leah, Nylund, Sven, Bel, Deborah Le, 2021. Moored turbulence measurements using pulse-coherent Doppler sonar. en *J. Atmos. Ocean. Technol.* 38 (9), 1621–1639. <https://doi.org/10.1175/JTECH-D-21-0005.1>. Publisher: American Meteorological Society Section: Journal of Atmospheric and Oceanic Technology issn: 0739-0572, 1520-0426.